Zandonadi *et al. Chem. Biol. Technol. Agric.* (2025) 12:71
https://doi.org/10.1186/s40538-025-00789-9

Chemical and Biological Technologies in Agriculture

RESEARCH

Open Access

Humic acids as drivers of plant growth: regulating root development and photobiology through redox modulation

Daniel Basílio Zandonadi[1*], Hiarhi Monda[2], Jason Gralian[2], Aletia James[2], Richard T. Lamar[2] and Mirella Pupo Santos[1*]

Abstract

Background Humic acids (HA) influence plant growth and development through various mechanisms that depend on the source and concentration of HA, as well as the specific plant organ and its developmental stage. Acting as biostimulants, these substances elicit stress-like responses and trigger physiological, biochemical, and molecular changes in plants that involve redox homeostasis. Therefore, we aimed to understand how purified HA derived from oxidized sub-bituminous coal impacts growth, redox states and photobiology in plants. After identifying the optimal HA dosage, plants were evaluated for their growth and photobiological responses, enzyme activities, reactive oxygen species (ROS) levels, and selected gene expression.

Results An HA concentration of 20 mg L^{-1} of carbon significantly enhanced most morphological and photobiological parameters. HA modulated the electron transport across the thylakoid membrane, thereby influencing the proton motive force and ATP synthesis. We also observed improved root growth within finer root diameter classes, which enhances foraging capacity and contributes to better nutrient absorption. HA stimulated fast ROS production, enhanced antioxidant enzyme activities, and increased H^+-ATPase activity in roots. In addition, HA induced the expression of the *roothairless5* (*rth5*) gene, which is involved in root hair growth. Furthermore, HA promoted the activity of H^+-ATPase, RBOH and NADH oxidases, and changed the expression of genes, such as *ZmSOD4*, *ZmCAT3*, *ZmPIN1b*, *ZmEXPA4*, *ZmLAX3*, *ZmHA2*, and *ZmTOR*.

Conclusions These findings suggest that HA promote plant development in roots by modulating oxidative stress through the RBOH/ROS/auxin/H^+-ATPase pathways while potentially influencing photobiological processes via their electron-donating and accepting properties. These effects may be attributed to the interplay between the pro-oxidant (e.g., quinones and semiquinone radicals) and the antioxidant functionalities (e.g., polyphenols) inherent in HA, both contributing to the observed eustress response. The coordinated action of the RBOH, H^+-ATPase, and TOR pathways likely help maintain a positive membrane oxidative balance, supporting root growth and development.

Keywords Humic substances, RBOH, H^+-ATPase, Expansins, Antioxidants, NADH oxidase, Auxin transport, Electron shuttle, Fine roots

*Correspondence:
Daniel Basílio Zandonadi
dz@ufrj.br
Mirella Pupo Santos
mirellapupo2020@gmail.com
Full list of author information is available at the end of the article

Graphical abstract

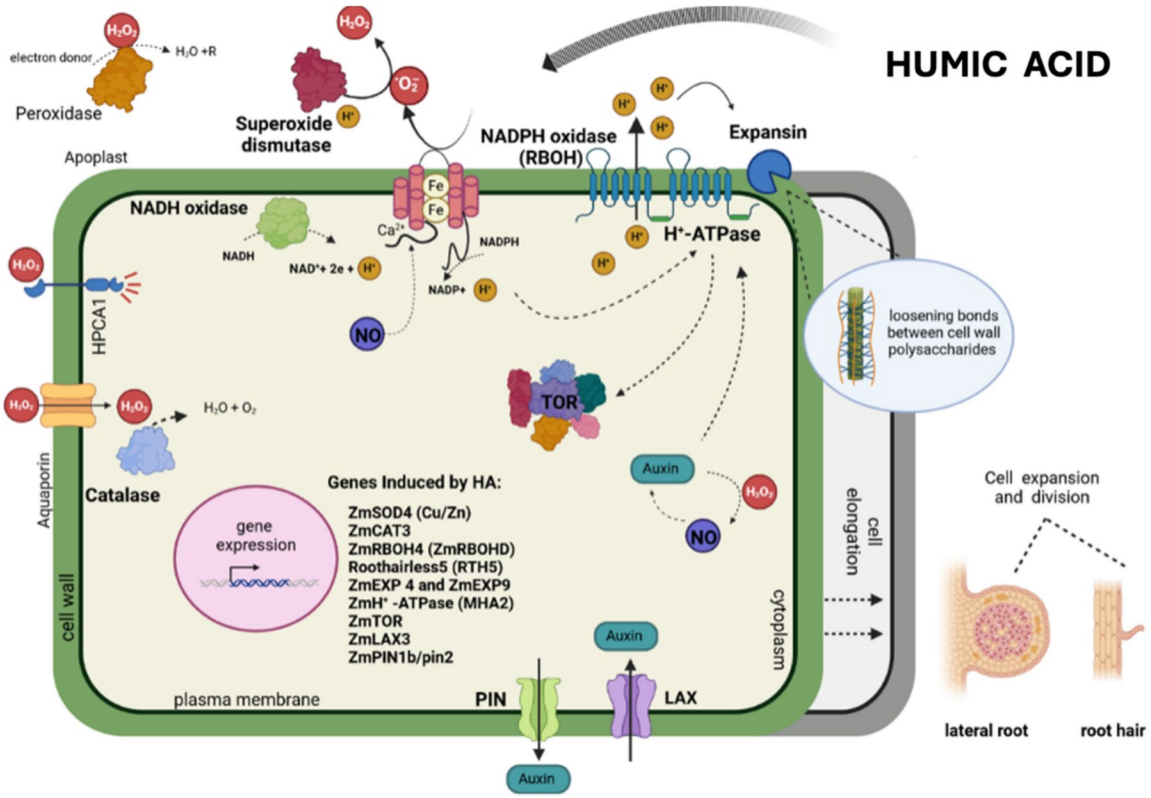

Background

Humic substances (HS) are formed through a series of chemical and biological transformations of plant and animal residues, as well as microbial metabolic byproducts, and represent the largest reservoir of organic carbon in the environment [1, 2]. Humic acids (HA), the principal alkaline-soluble fraction of HS, function as key plant biostimulants and are commercially sourced from brown lignite, oxidized lignite (e.g., leonardite), and oxidized sub-bituminous coal [3, 4]. Humic acids enhance plant biomass accumulation and crop productivity by promoting nutrient acquisition and improving abiotic stress tolerance, thereby supporting sustainable agricultural practices [2, 5].

Numerous studies have explored the role of specific functional groups within their structure in influencing plant growth, both directly and indirectly [3, 6]. However, the specific chemical mechanisms of HA responsible for their biostimulant effects on plants remain unclear. Despite the promising agricultural potential of HA, its commercial application must consider appropriate concentration levels, as excessive amounts, depending on the humic source, plant species, organ type, and developmental stage, can become phytotoxic [4, 7].

The oxidation–reduction (redox) state of cells integrates external and environmental signals into intracellular metabolism through the action of plasma membrane enzymes, such as NADH and NADPH oxidases. These enzymes are responsible for transmembrane electron transport from the cytoplasm to the apoplast via reduced NAD [8] and NADP [9], respectively. The NADH oxidases are induced by natural and synthetic auxins [10, 11], quinones and ferrous ions [12]. These enzymes are correlated with both pH and ion gradients in the cell [12] and are thought to play a critical role in elongation growth through control of plasma membrane extension [13]. NADPH oxidases, also known as plant respiratory burst oxidase homologs (RBOH), are calcium-dependent NADPH oxidases. These enzymes regulate reactive oxygen species (ROS) generation in processes, such as cell wall elongation, root hair growth, pollen tube development, and plant reproduction [14, 15]. Similar to the

RBOH found in mammalian neutrophils (NOX), these enzymes play crucial roles in ROS production during various developmental stages and plant–microbe interactions [16]. In *Zea mays*, at least 15 RBOH genes have been identified, each expressed in specific tissues and involved in various plant functions [17].

The cellular redox state can fluctuate between diurnal and nocturnal cycles and is influenced by environmental conditions [18]. These redox changes affect growth and development [19], with the balance of ROS being regulated by the antioxidant system [20]. ROS, such as hydrogen peroxide (H_2O_2), and reactive nitrogen species (RNS), such as nitric oxide (NO), play essential roles in plant signaling at low concentrations, participating in various pathways, including those mediated by hormones [21]. Abiotic stressors trigger a Ca^{2+} flux from apoplast to cytoplasm that directly activates RBOH when Ca^{2+} binds to RBOH EF-hand motifs which, along with phosphorylation of the enzyme, leads to apoplastic superoxide (O_2^-) and finally H_2O_2 production [19, 22]. The accumulation of apoplastic H_2O_2 is sensed by adjacent cells which triggers a Ca^{2+} flux into these cells, which activates their own RBOHs, thus generating a systemic stress response [23]. Some ROS and RNS species, such as H_2O_2, can oxidize cysteine residues in proteins, altering their structure, activity, and/or stability through electron transfer [24–26]. Among the proteins susceptible to oxidation are enzymes but also transcription factors. Consequently, ROS can influence cellular functions by modifying signaling pathways as well as transcriptional and post-transcriptional responses [27].

The most widely accepted hypothesis regarding how HA modify plant physiology centers on the regulation of plant bioenergetics [6, 28]. This includes the elicitation of a mild stress or beneficial (i.e., eustress) response, similar to that described for abiotic stress [3]. This response involves increased ATP production at key stages of metabolic pathways, such as glycolysis and the citric acid cycle, thereby providing more energy for proton pumps to facilitate ion uptake and support growth through both auxin-dependent and independent pathways [28–32]. Given the importance of photosynthesis in energy production and the known effects of HA on glycolysis and the tricarboxylic acid cycle [28], it is reasonable to expect extensive research into how HA regulates photosynthesis. While HA have been shown to increase ROS in plants and induce antioxidant responses [33], the precise mechanisms by which HA influences cellular redox states remain poorly understood. Given that the cellular redox state is closely linked to several critical plant processes, including photosynthesis, this study aims to deepen our understanding of how HA and their chemical structures promote root growth and influence photobiological changes by inducing alterations in the cellular redox state. We hypothesize that HA activates the enzyme RBOH, leading to transient oxidative stress, which is subsequently mitigated by cellular antioxidant responses. The mode of action of HA, therefore, involves altering the cellular redox state, modulating photobiological processes and which subsequently promotes root growth and development.

Methods

Extraction of humic acids

The HA used in this study was extracted and purified from a Cretaceous oxidized sub bituminous coal (i.e., humate ore) from a seam in New Mexico. The extraction and purification procedures followed those outlined in [34]. Briefly, 2.5 g of humate ore were extracted in 1 L of 0.1 M NaOH for 6 h under a N_2 atmosphere. After extraction, the alkaline extract was centrifuged at 5250 g for 2 h to separate the HS-containing alkaline supernatant from the insoluble materials. The pH of the alkaline extract was then adjusted to pH 1 using 11.7 M HCl to precipitate the HA. After complete precipitation, the pH-adjusted extract was then centrifuged again at 5250 g for 2 h. At the end of centrifugation, the fulvic fraction-containing supernatant was decanted off. The humic precipitate was then transferred to 250 mL centrifuge tubes and de-ashed by washing with a dilute HCl/HF solution [(5 mL of 11.7 M HCl + 5 mL of 27.6 M HF) L^{-1}]. After HCl/HF treatment, the tubes were centrifuged at 5250 g for 1 h and the original HCl/HF solution was replaced with 200 mL of fresh HCl/HF solution. This process was then repeated twice using deionized H_2O with the pH adjusted to pH 1 with 11.7 M HCl. After the final centrifugation, the acidified deionized H_2O was decanted and the purified HA was frozen at -80˚C, lyophilized and stored in a sealed glass vial until use.

Chemical analysis of humic acids: fourier transform ion cyclotron resonance mass spectrometry (FT-ICR MS)

A custom-built 9.4 T FT-ICR mass spectrometer at the National High Magnetic Field Laboratory, equipped with a horizontal, 220 mm bore diameter, and operated at room temperature, was used to analyze the HA sample. A modular ICR data station (Predator 32) was used for instrument control, data acquisition, and data analysis [35, 36] [7, 35]. The HA sample was first dissolved in 7.5 M NH_4OH, followed by double dilution with MeOH:H_2O (1:1) to a concentration of 100 mg L^{-1} [37]. NH_4OH was used to solubilize the dried HA and to increase the ionization efficiency in the ESI source, while MeOH was used to better affect the charge distribution and stability of the formed ions. The mass spectrum was acquired in negative ionization mode with an

introduction flow rate of 0.5 µL min^{-1}, ESI needle voltage of − 3,000 V, 100 scan accumulation, and 400 ms event length. 100 individual transients of 5.8–6.1 s duration collected for crude extract were averaged, apodized with a Hanning weight function, and zero-filled once prior to fast Fourier transformation. Mass peaks with S/N > 6 were processed for formula assignment using the National High Magnetic Field Laboratory PetroOrg© software by setting the following parameters: ^{12}C 1−100, ^{1}H 2−200, ^{16}O 2−30, ^{14}N 0−3, ^{32}S 0−3 with a mass error threshold ≤ 0.5 ppm. Formulae with the least N and S were assigned first [40]. Generated formulae were filtered by O/C ratio (≤ 1) and H/C ratio (≤ 2) according to Koch et al. (2005) [37]. The degree of hydrogen and oxygen saturation and molecular heterogeneity were assessed within the assigned formulae and molecular reactivity analyzed based on H/C and O/C ratios by means of a Van Krevelen diagram [38] whose molecular compositional space was divided into the typical classes of discrete organic biomolecules found in organic matter according to the following rules: (1.5 < H/C < 2; O/C ≤ 0.3) lipid-like, (1 < H/C < 2.2; 0.1 < O/C < 0.67; N ≥ 1) protein-like, (0.7 < H/C < 1.5; 0.1 < O/C < 0.67) lignin-like, (H/C > 1.5; O/C > 0.67) carbohydrate-like, (0.2 < H/C < 0.7;O/C ≤ 0.67) CAS Condensed aromatic structures, (0.7 < H/C < 1.5; O/C ≤ 0.1) UHC Unsaturated hydrocarbon.

Dose response curve

To determine the optimal range for HA treatment, we conducted a 2 week corn bioassay. For 2 week assays, 30 seeds were germinated in individual pots (2 seeds in each of 15 pots) with vermiculite substrate soaked in deionized H_2O. At 4 days after seeding, each pot was thinned to retain one uniform plant per pot. These 15 uniform plants per treatment were placed in trays to which the treatments and control were added. The concentrations tested were 0, 10, 20, 30, and 40 mg L^{-1} of carbon. The HA treatments and the control both received half-strength Hoagland's solution. The HA stock solution was prepared according to [31]. Briefly, the purified HA powder was dissolved into 250 mL of Tris buffer (pH 10, 0.1 M). After dissolving in Tris buffer, 1750 mL of 57% Hoagland's solution was added, and the stock (pH 7.0) was stable with no precipitation for several months. Two liters of each treatment solution (pH range 5.8–6.0) were applied to their respective trays immediately after thinning. The solution was immediately absorbed by the vermiculite, and any remaining solution on the tray was checked daily for HA precipitation. For the evaluation of corn root morphology in both experiments, we evaluated the total root length (TRL), root surface area, total root average diameter, and TRL of the 0–0.25 mm diameter root class using scanned images analyzed with WinRHIZO™ software (Regent Instruments Inc.). The photobiology and statistical analyzes are described below.

Experiments with the optimum HA concentration

After analyzing the dose–response experiments, a concentration of 20 mg L^{-1} of carbon was determined to be the optimal rate. Consequently, three additional experiments were conducted to assess growth through biometric and photobiological measurements, as well as the biochemical and molecular responses to HA treatment. In each experiment, 20 plants were grown and treated following the protocol described before. Of these, 10 plants per treatment were used for biometric and photobiological analyses, while the remaining 10 were allocated for biochemical and molecular analyses. The experiments were repeated three times, resulting in a total of 30 samples for biometric and photobiological assessments, and 15 for biochemical and molecular analyses.

Photobiology and biometric analysis

To investigate whether HA influenced the light reactions of photosynthesis, several photosynthetic parameters were measured to explore the potential causal relationship between root-applied HA and its effects on chlorophyll *a* fluorescence. Plants were harvested at V5, and we analyzed the photobiology at the 4th leaf during the late afternoon (in the last 2 h of the photoperiod). Corn photosynthesis was evaluated using the handheld fluorometer MultiSpeQ V 2.0 with the PhotosynQ platform (www.photosynq.com) according to [39]. The protocol Photosynthesis RIDES 2.0 was used to measured chlorophyll *a* fluorescence effective quantum yield (Phi2 or Φ2), non-photochemical quenching (ΦNPQ), the redox state of quinone A (qL), and chlorophyll index (SPAD value). The electrochromic shift ECS_t is the magnitude of the light-induced *pmf* and was used to estimate thylakoid proton conductivity via ATP synthase (g_H^+) using DIRK (dark-interval relaxation kinetics) analysis. The plants were subjected to the same photosynthetically active radiation (PAR) during the entire experiment and light reactions measurements.

In the same experiment, after photobiological analysis, the roots were collected for measurements of total root length, root surface area, root average diameter, root volume, and the number of lateral roots using WinRHIZO™ software (Regent Instruments Inc.). Fresh weight samples of the roots were then measured using a precision balance.

Biochemistry analysis

Plasma membrane enzyme activities

The microsomal fraction (plasma membrane and tonoplast) was then used to measure the activity of H^+-ATPase, NADPH oxidase (RBOH), and NADH oxidase using specific inhibitors and substrates. The microsomal fraction was isolated from plant material using differential centrifugation, as described by [30]. The tissue was homogenized in a cold extraction buffer with a porcelain mortar (1:2 g/mL) 24 h after HA treatment. The extraction buffer was composed of 250 mM sucrose, 10% glycerol, 100 mM tris-base, 5 mM EDTA (or EGTA), 100 mM KCl, 5 mM DTT, 1 mM PMSF, 0.4% PVP-40 T 1%, 0.3% BSA. The pH was adjusted to pH 8 with 1,3-bis[tris(hydroxymethyl)methylamino]propane (BTP). The homogenate was filtered through two layers of Miracloth (Calbiochem, cat. no. 475855-1R). The extract was centrifuged at 3000×*g* for 15 min at 4 °C. The supernatant was centrifuged again at 10000×*g* for 15 min at 4 °C followed by a second centrifugation. Next the supernatant was centrifuged, a third time, at 32000*g* for 40 min to separate the microsomal fraction. The precipitate from this third centrifugation was resuspended in a buffer solution containing 10% glycerol, 100 mM MOPS (pH 7.6), 2 mM EGTA, 2 mM DTT and PMSF (1 mM) and $MgSO_4$ (3 mM), benzamidine (1 mM). The resuspended and homogenized pellet was stored at − 80 °C. All enzymatic activities were calculated based on the protein content per sample, which was determined according to [40].

The plasma membrane H^+-ATPase activities were determined using microsomal fractions by colorimetrically assay for determination of Pi released during ATP hydrolysis, according to the method described by [41], with modifications proposed by [30]. Specific inhibitors to plasma membrane H^+-ATPase (i.e., vanadate) was used to detect the specific activity of the enzyme.

The plasma membrane protein fractions used for measuring NADPH (RBOH) and NADH oxidase activities were isolated as previously described. RBOH activity was measured according to the method of [42]. The reaction medium contained 50 mM TRIS–MES buffer (pH 7.4), 0.2 mM XTT, 0.2 mM NADPH, and 15 mg of membrane proteins. The reaction was initiated by adding NADPH. The assay was performed both with and without 200 µM diphenyleneiodonium (DPI), which was used to inhibit RBOH-like enzyme activity and to determine possible NADPH oxidation by the NADH oxidase. XTT reduction was monitored by measuring absorbance at 470 nm. Corrections for background activity were made by including 50 units of superoxide dismutase (SOD). The NADH oxidase assay was conducted as described by [43], using a reaction medium containing 50 mM TRIS–MES buffer (pH 7.0), 150 µM NADH, and 10 mg of plasma membrane proteins. The reaction was initiated by adding NADH, and the specific activity of the plasma membrane was calculated using an NADH extinction coefficient of 6.2 mM^{-1} cm^{-1}. Diphenyleneiodonium (200 *u*M) was used to inhibit RBOH-like enzyme activity.

ROS and nitric oxide content and antioxidant

The accumulation of reactive oxygen species (ROS), such as superoxide ($O_2^{ï-}$) and hydrogen peroxide (H_2O_2), as well as nitrogen species, nitric oxide (NO), was measured at 0, 15, 30, and 60 min after treatment with 20 mg L^{-1} of carbon of HA. Plant roots were collected and immediately frozen in liquid nitrogen until further processing. Superoxide content was measured using the Inhibition and Production of Superoxide Colorimetric Assay Kit (Elabscience). The H_2O_2 content was determined using a Peroxidase Assay Kit (Sigma-Aldrich, MAK311) and NO using a NO Assay Kit (Sigma-Aldrich, MAK454), all following the manufacturers' protocols.

Antioxidant capacity was assessed using the Total Non-Enzymatic Antioxidant Capacity Assay Kit (Sigma-Aldrich, No. MAK187), following the manufacturer's instructions. Leaf tissues (0.05 g) from each condition were pooled and homogenized in 100 mL of water, centrifuged at 15,000 g for 1 min, and the supernatant was collected. A copper solution was then added to the supernatant, and the samples were incubated at room temperature for 90 min. The antioxidant capacity was measured using a Synergy/HTX Biotek Multi-Mode Reader at 570 nm.

The catalase activity assay was performed using the Catalase (CAT) Activity Assay Kit (Elabscience), while the superoxide dismutase (SOD) activity was measured using the Total Superoxide Dismutase (T-SOD) Activity Assay Kit (Elabscience). Sample preparation and enzyme activity measurements followed the protocols provided by the manufacturer.

Molecular analysis

The primers for the gene sequences from NCBI were designed using NCBI tools and Primer3Plus program. The primer sequences were analyzed using the Oligo-Analyzer Tool for stability and unwanted pairing. The best primers were synthesized and tested on a 1% agarose gel through electrophoresis, applying a voltage of 75 V for approximately 50 min in 1X Tris/Borate/EDTA (TBE) buffer, to confirm the presence of a single band after PCR amplification using cDNA. The PCR configuration included incubation at 25 °C for 10 min, 37 °C for 120 min, denaturation at 85 °C for 5 s, and storage at 4 °C until further analysis. The sequences utilized in

this study were retrieved from the National Center for Biotechnology Information (NCBI) Database [https://www.ncbi.nlm.nih.gov/] and the Maize Genetics and Genomics Database (MaizeGDB) [http://www.maizegdb.org/expression/]. All sequences are included in Supplementary Table 1.

Roots samples were collected for total RNA extraction from a combined sampling of 9 plants per treatment, divided into triplicates (3 plants per replica). The experiments were repeated three times, resulting in a total of 9 samples per treatment. Plant roots (500 mg) were ground with liquid nitrogen in ceramic mortar and pestle, and 5 mL of Tri Reagent® (Sigma-Aldrich T9424) was added to the samples, followed by a 5 min incubation at room temperature. The samples were then centrifuged at 4 °C for 5 min (12,000 g), and the upper aqueous phase was transferred to a new tube, where 200 µL of chloroform was added. The tubes were manually shaken for a few seconds and incubated at room temperature for 5 min. A second centrifugation step was performed for 15 min (12000*g*) at 4 °C. The RNA was recovered from the supernatant and reacted with 1 mL of isopropanol in a new tube for precipitation. The samples were stored in a freezer at − 20 °C for approximately 1 h to enhance extraction efficiency. The tubes were centrifuged at 4 °C again for 15 min (15000*g*), and the supernatant was discarded. Then, 1 mL of 12 M ethanol was added to each tube for sample purification, followed by a final centrifugation at 4 °C for 5 min (15000*g*). After discarding the ethanol and drying the tubes, the RNA was resuspended in 30 µL of endonuclease-free ultrapure water and incubated in a water bath at 60 °C for 15 min. RNA quality was analyzed using a 5 g/kg agarose gel electrophoresis, subjected to a voltage of 100 V and a current of 400 mA for approximately 20 min in 1X Tris–Acetate-EDTA (TAE) buffer. RNA quantification was performed using a NanoDrop 2000c spectrophotometer (ThermoFisher Scientific). Once the quality of the extracted RNA was confirmed, complementary DNA (cDNA) synthesis was performed using 2 µg of RNA with the high-capacity cDNA reverse transcription kit (applied biosystems). For this, 10 µL of the reaction mix and 10 µL of each sample were mixed and placed in a thermocycler with the following configuration: 25 °C for 10 min, 37 °C for 120 min, 85 °C for 5 min, and 4 °C until the cDNA samples were retrieved. The cDNA samples were stored at − 20 °C in the freezer for future gene expression analysis.

Quantitative real-time reverse transcript amplification analyses were performed in a StepOnePlusTM thermocycler (Applied Biosystems) from total cDNA derived from RNA samples. Amplifications were carried out in initial incubations at 95 °C for 10 min, followed by 40 cycles of 95 °C for 15 s and 1 min at 60 °C. After the reaction cycles, the determination of the dissociation curves of each product (melting curve) at a temperature of 95 °C for 15 s, 60 °C for 1 min, and again at 95 °C for 15 s. Relative expression was calculated with amplification Ct values using the delta–delta Ct methodology [44] was used to quantify relative gene expression with *ZmTUA4* and *ZmGAPDH* as internal controls.

Statistical analysis

Data were analyzed for residual normality and homoscedasticity using the D'Agostino–Pearson omnibus test. Data presenting a normal distribution was submitted to analysis of variance (ANOVA) followed by test of Tukey or Dunnett for different HA concentrations. Afterward, only the lower HA concentration able to change plant growth and photosynthesis, was tested against the control, and the statistical significance was measured using the t test. All statistical calculations were performed with GraphPad Prism version 10.3.1 for Mac, GraphPad Software, Boston, Massachusetts USA.

Results

Fourier transform ion cyclotron resonance mass spectrometry of HA

The FT-ICR MS analysis produced 9.902 peaks assigned to a molecular formula. The compounds not assigned to a molecular formula represent 0.10% of the total (No hit). The total weighted average of the molecular weights was 403 m/z with an average of 23 C atoms and 18 equivalent

Table 1 Group distribution and molecular descriptors of HA FT-ICR MS spectrum upon formula assignment

	Rel. Ab	m/z avg	A.W. avg DBE	A.W. avg C#	Median C #	median H/C	median O/C	Avg AI
CHO	Ox (41.6%)	413.5	18.8	25.3	28	0.76	0.21	0.61
	Ox13Cy (7.67%)	410.8	18.7	24.2	24	0.04	0.22	0.67
CHON	NxOy (41.28%)	432.3	20.4	25.8	27	0.61	0.21	0.7
	NxOy13Cz (6.95%)	425.6	20.3	24.7	24	0.04	0.21	0.76
CHOS	OxSy (2.24%)	372.8	15.7	20.4	19	0.63	0.06	0.68
	OxSy13Cz (0.16%)	364.3	16	19.7	20	0.05	0.05	0.81

double bonds (DBE) (Table 1). Upon grouping by heteroatomic composition, it was found that CHO and CHON formulas had the highest occurrence, accounting for 49.3% and 48.2% of the total peaks, respectively, followed by CHOS (2.4%). In contrast, no CHONS formulas were identified (Table 1). The smaller molecular weight formulas belonged to the CHOS group, the less represented group. However, the molecular weight in the CHO and CHON groups did not exceed 425.6 m/z. The presence of small molecules across the groups with a low molecular weight suggests a dynamic behavior of the HA, where the presence of weak dispersive forces leads to the formation of supramolecular dynamic aggregations.

The Van Krevelen diagrams shown in Fig. 1 visually describe the molecular distribution according to the superimposed or singular heteroatomic group. The area defined by the low H/C and O/C ratio is where most of the molecules were concentrated for both CHO and CHON formulas, suggesting the very aromatic character of the oxidized sub-bituminous coal HA. CHOS molecules were mainly spread along the *y*-axis and showed a very small content of oxygen. Specific values of hydrogen-to-carbon (H/C) and oxygen-to-carbon (O/C) ratios were used to define regions, where distinct classes of organic compounds, including lignin, lipids, proteins, carbohydrates, condensed aromatic structures (CAS), and unsaturated hydrocarbons (UHC) can be located. By following this approach, the percentage of molecules per class of organic compounds was calculated as well as the contribution of each heteroatom group per class, as shown in Fig. 2. As expected, most of the molecules belonged to CAS and lignin classes, followed by UHC, lipid, and protein. No carbohydrates were found. The composition of biomolecule groups in terms of heteroatom classifications showed that CHO formulae were mostly associated with lipids (89.7%), lignin (50.5%), and CAS components (35.5%) (Fig. 2B). In contrast, CHON formulas were distributed more evenly between CAS (54.4%) and lignin compounds (45.7%), with a smaller presence in UHC (37.7%). CHOS formulae were mainly observed in UHC. The relatively most abundant formulas per each biomolecule group were investigated online by referencing databases such as PubChem and chEMBL to attempt the identification of the molecules (Supplementary Table 2). The most representative molecules belonged to the CAS and lignin groups and are indicative of highly conjugated

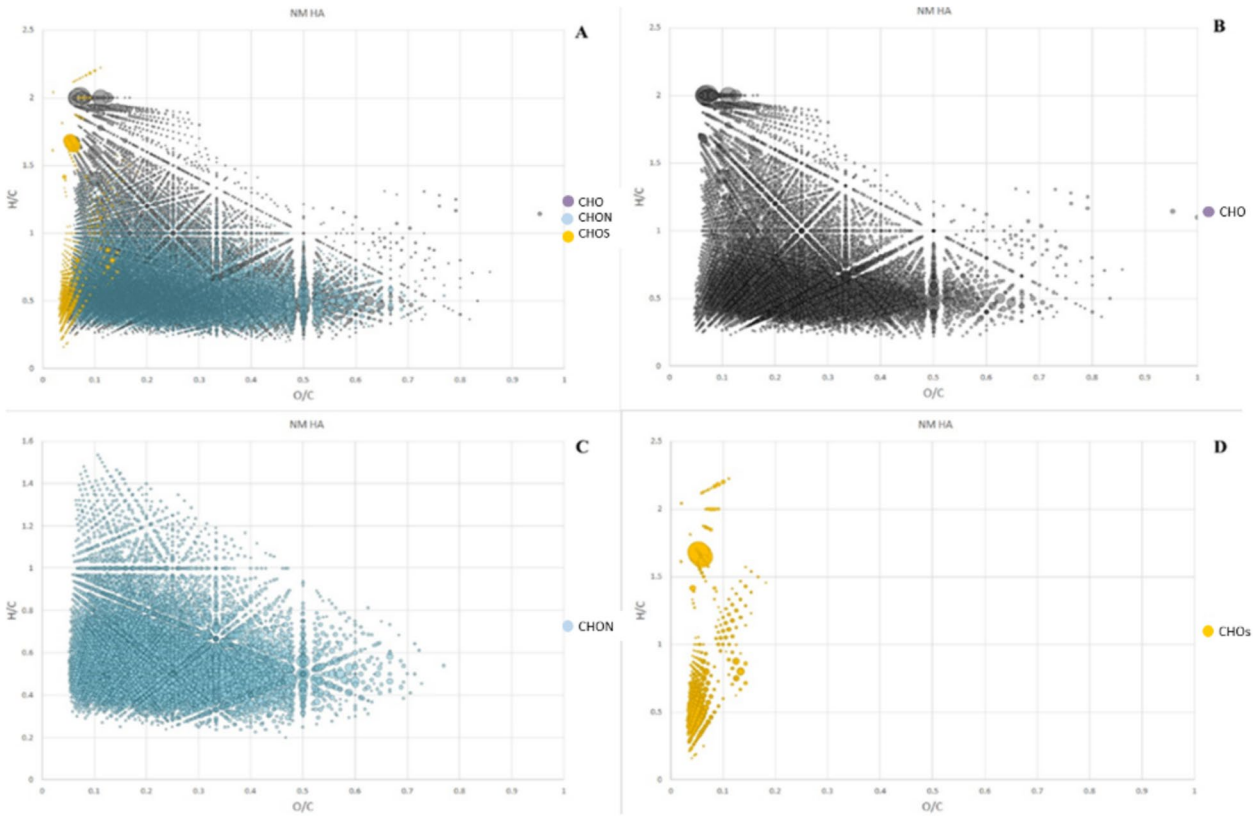

Fig. 1 Van Krevelen diagram of all molecules assigned to a molecular formula (**A**), and grouped according to the heteroatom composition, CHO (**B**), CHON (**C**), CHOS (**D**)

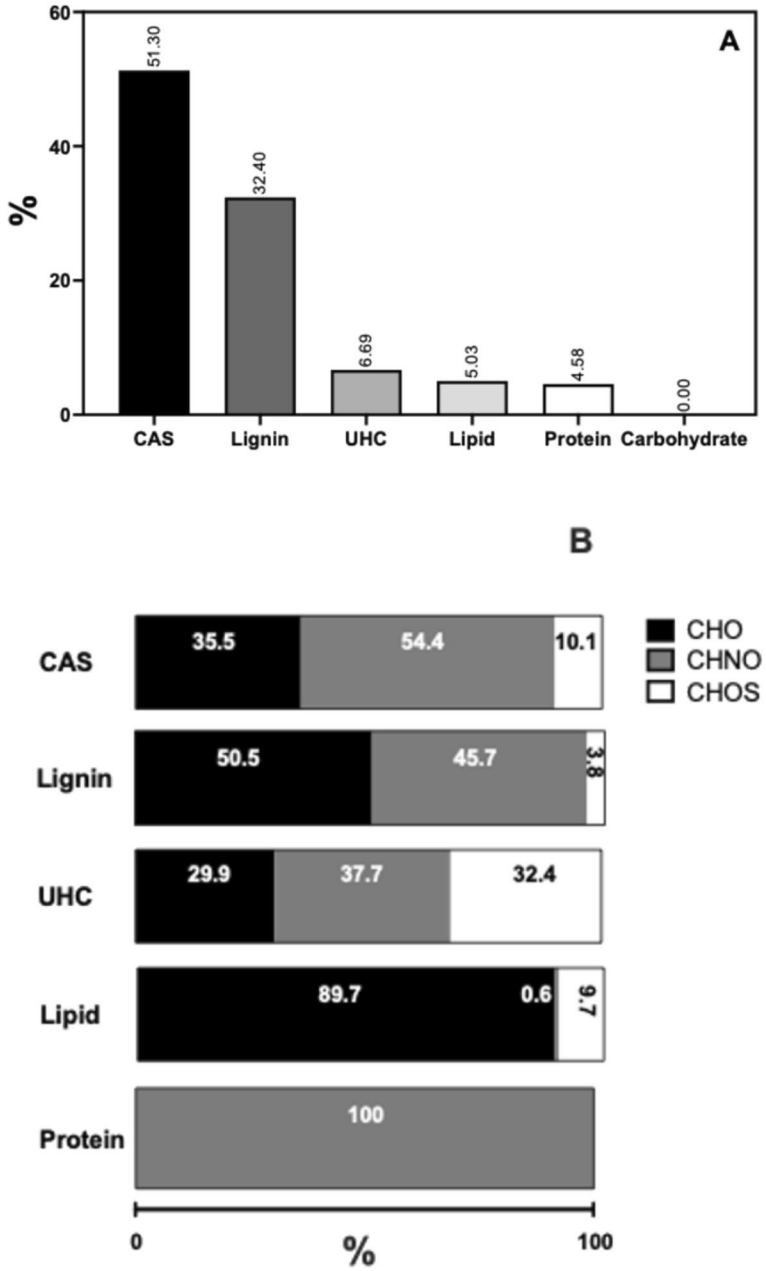

Fig. 2 **A** Biomolecule class distribution in the entire cluster of identified molecules; **B** each biomolecule class composition according to the heteroatom group classification. *CAS* condensed aromatic structures. *UHC* unsaturated hydrocarbons

polycyclic aromatic quinone, phenolic, and heterocyclic systems. The most abundant CAS-assigned molecular structures are quinone and anthraquinone derivatives of fungal and microbial origin often showing biological activity (e.g., preussomerin, eucapsitrione, hypericin, and oviedomycin). In contrast, lignin-derived formulae appear to contain structural features characteristic of flavonoids, such as the flavone backbone (e.g., 3-hydroxy-4-(3-oxo-3-phenylpropanoyl) phenyl benzoate), where the presence of specific substituents such as the acetyl or the hydroxyl group (e.g., Di-acetyl flavone and 3-acetoxyflavone) might play an important role in shaping the molecule chemical properties and behavior.

Dose response experiment

We observed that above 20 mg L^{-1} of carbon (equivalent to 34 mg HA/L) there was an increase in total root length and in the fine root length class diameter (around 70%)

while a reduction of 89% in root diameter average (Supplementary Fig. 1). The dose–response curve test for the photobiological parameters also indicated a consistent change above 20 mg L^{-1} of carbon treatment (Supplementary Fig. 1). This concentration was the lowest concentration that consistently demonstrated a statistically significant positive effect across all measured parameters. Therefore, the 20 mg L^{-1} of carbon concentration was chosen for further experiments.

Experiments with the optimum HA concentration

Photobiology and biometric analysis

The results showed that HA treatment (20 mg L^{-1} of carbon) improved Phi2 (effective quantum yield) by 12% (Fig. 3A), qL value (redox state of quinone A) by 15% (Fig. 3C), and ETR by 12% (Fig. 3D), while NPQ (non-photochemical quenching) decreased by 20% (Fig. 3B). The electrochromic shift (ECSt), SPAD values and thylakoid proton conductivity via ATP synthase (g_{H}^{+}) increased by approximately 55% (Fig. 3E–G). This demonstrates that HA can alter relative light-driven proton flux, influencing the electric flow across the thylakoid membrane, affecting proton motive force (ECSt), and ATP synthesis (gH^{+}) (Fig. 3F, G).

Humic acids improved total root length by 55% (Fig. 4A) and root surface area by 30% (Fig. 4B). HA reduced average root diameter by 12% (Fig. 4C) and increased root volume by 22% (Fig. 4D). In addition, HA increased the number of lateral roots by 85% (Fig. 4F) and total root fresh weight by 33% (Fig. 4E). These changes improve root foraging capacity, such as increased surface area and finer root structures.

Biochemistry analysis

Plasma membrane enzyme activities

H^{+}-ATPase activity increased by 65% after 1 h of HA exposure, and this activity remained higher than the control after 24 h (64%) (Fig. 5A). NADH oxidase activity increased by 64% after 1 h compared to control plants

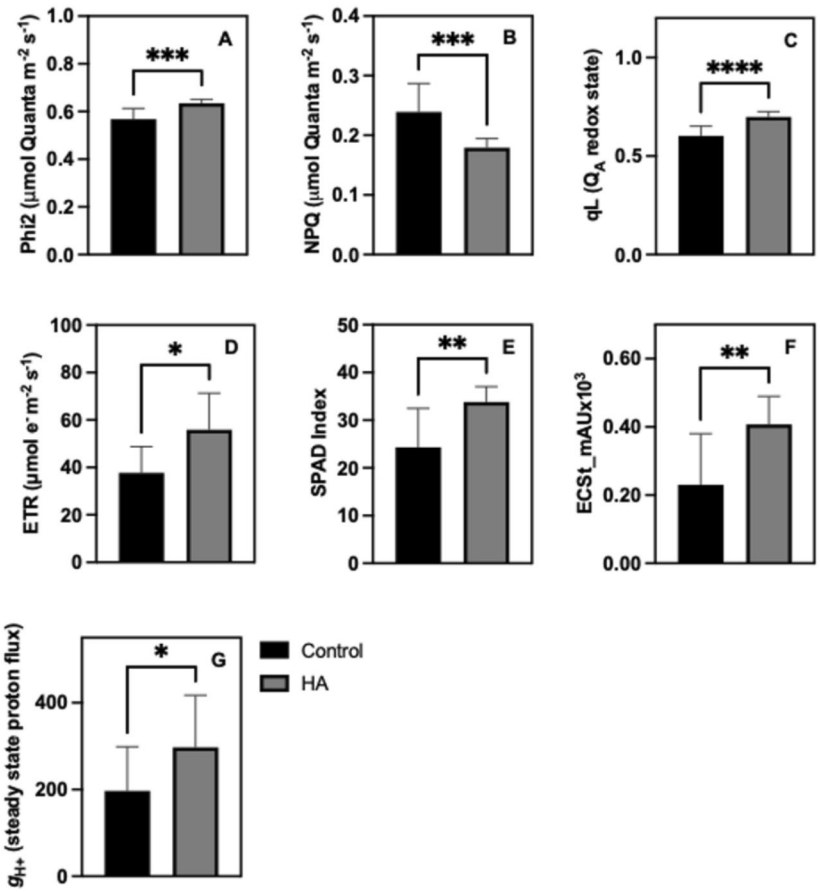

Fig. 3 Photobiology responses to HA treatment after 7 days. **A** Effective quantum yield (Phi2 or Φ2); **B** non-photochemical quenching (ΦNPQ); **C** redox state of quinone A (qL); **D** electron transport rate (ETR); **E** chlorophyll index (SPAD index); **F** magnitude of electrochromic shift (ECSt); **G** thylakoid proton conductivity via ATP synthase (g_{H}^{+}). Asterisks indicate significant differences according to *t* test (*P < 0.05, **P < 0.01, ***P < 0.001, ****P < 0.0001, ns = not significant)

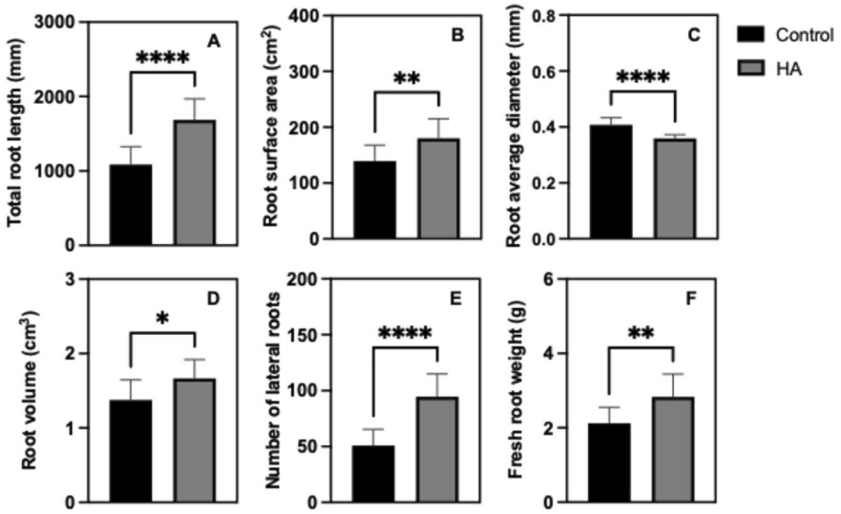

Fig. 4 Root architecture responses to HA treatment after 7 days. **A** Total root length; **B** root surface area; **C** root average diameter; **D** root volume; **E** number of lateral roots; **F** fresh root weight. Asterisks indicate significant differences according to *t* test (*P < 0.05, **P < 0.01, ***P < 0.001, ****P < 0.0001, ns = not significant)

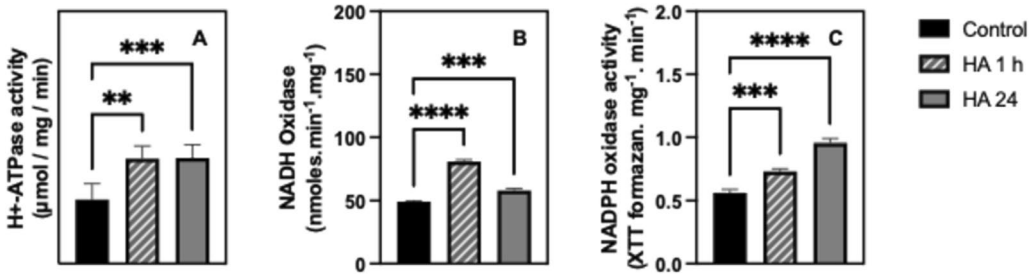

Fig. 5 Plasma membrane enzyme activities responses to HA treatment in root tissue after 1 h and 24 h. **A** Plasma membrane H^+-ATPase; **B** NADH oxidase; (**C**) NADPH oxidase or RBOH. Asterisks indicate significant differences according to Dunnett's test (*P < 0.05, **P < 0.01, ***P < 0.001, ****P < 0.0001, ns = not significant)

and showed a less pronounced increase of 18% after 24 h (Fig. 5B). Root NADPH oxidase (RBOH) enzyme activity increased by 30% after 1 h compared to control and showed an even greater increase of 71% after 24 h exposure (Fig. 5C).

ROS and nitric oxide content and antioxidant

THA triggered the production of ROS and NO (Fig. 6). Superoxide accumulation in roots increased significantly, with a rise of 155% at 15 min and 143% at 30 min following HA treatment (Fig. 6A); however, the concentration decreased after 1 h. A similar pattern was observed for NO, which increased by 20% at 15 and 30 min after HA treatment. After 1 h, there was a reduction in NO concentration to levels similar to untreated plants (Fig. 6C). In contrast, H_2O_2 levels in HA-treated plants showed a notable increase only at the 30-min mark, increasing up to 90% when compared to non-treated plants (Fig. 6B). Superoxide dismutase (SOD) activity was enhanced by 50% to 84% several hours after HA exposure (at 5 and 24 h) (Fig. 6D). Meanwhile, HA treatment induced catalase (CAT) activity at all observed timepoints, with increases ranging from 70 to 127% (Fig. 6E). In addition, the total antioxidant capacity (non-enzymatic) increased by 26% (Fig. 6F).

Molecular responses: gene expression

Humic acids treatment led to significant changes in gene expression. Specifically, after 24 h, the transcripts of all genes were upregulated including, *ZmPHT1* (2.7-fold) (Fig. 7A), *ZmNRT2.1* (1.8-fold) (Fig. 7B), *ZmPIN1b* (1.7-fold) (Fig. 7C), *ZmLAX3* (1.6-fold) (Fig. 7D), *ZmEXPA4* (1.5-fold) (Fig. 7E), *ZmEXPA9* (1.7-fold) (Fig. 7F), *ZmHA2* (1.6-fold) (Fig. 7G), *ZmTOR* (1.5-fold) (Fig. 7H), *Zmrth5* gene (1.5-fold) (Fig. 7I), *ZmRBOH4* (1.5 fold) (Fig. 7J), *ZmSOD4 Cu/Zn* (2.5-fold) (Fig. 7K) and *ZmCAT3* (twofold) (Fig. 7L). Furthermore, humic acids-treated plants exhibited higher transcription levels of

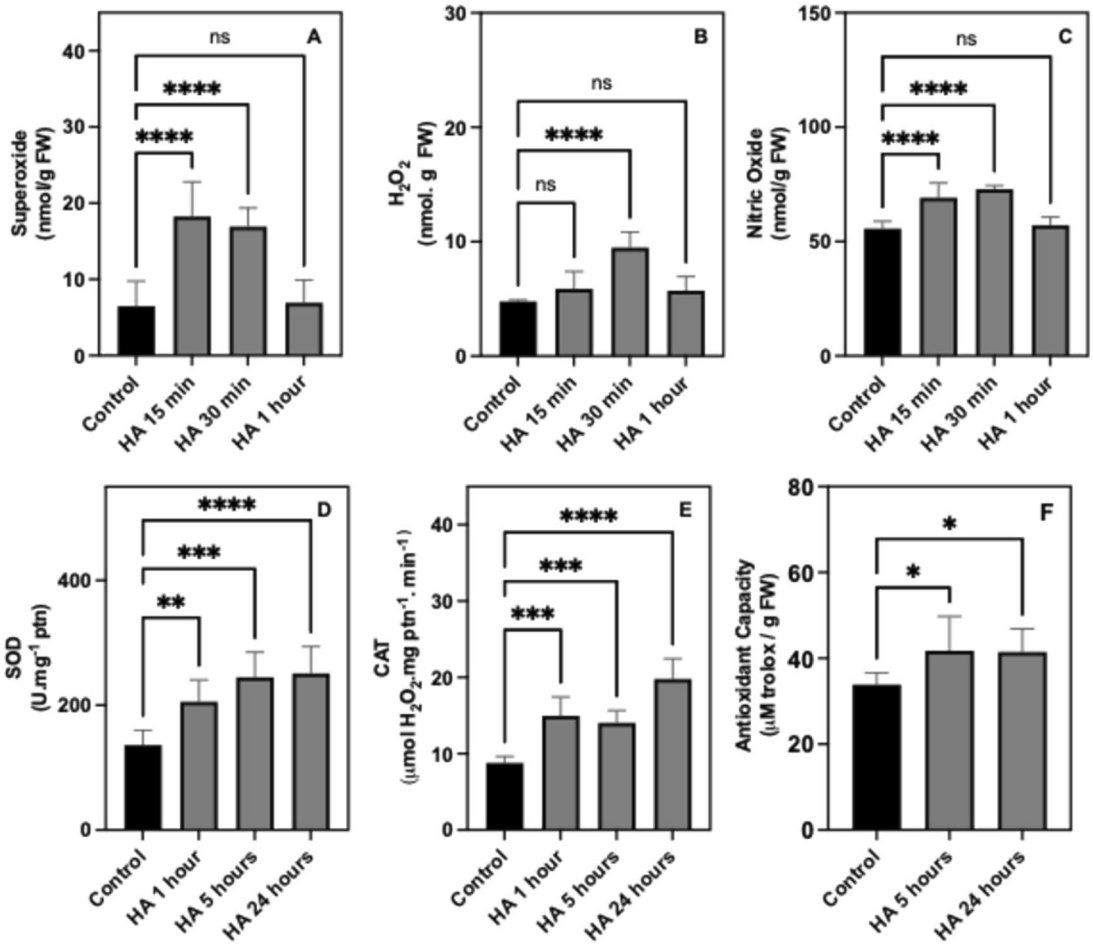

Fig. 6 ROS and Nitric oxide content and Antioxidant responses to HA treatment in root tissue. **A** Superoxide content; **B** peroxide content; **C** nitric oxide content; **D** superoxide dismutase activity; **E** catalase activity; **F** total antioxidant capacity (non-enzymatic). Asterisks indicate significant differences according to Dunnett's test (*P < 0.05, **P < 0.01, ***P < 0.001, ****P < 0.0001, ns = not significant)

several genes after 7 days compared to untreated plants. The induced genes included *ZmH*$^+$*-ATPase2* (1.3-fold) (Fig. 7G), *ZmTOR* (1.5-fold) (Fig. 7H), *Zmrth5* (1.6-fold) (Fig. 7I), *ZmRBOH4* (1.5-fold) (Fig. 7J), *ZmSOD4* Cu/Zn (1.6-fold) (Fig. 7K), and *ZmCAT3* (1.6-fold) (Fig. 7L). However, some genes were downregulated including *ZmNRT2.1* (0.4-fold) and *ZmLAX3* (0.5-fold) (Fig. 7B, D). The genes *ZmPHT1*, *ZmPIN1b*, *ZmRBOH4, ZmEXPA4, ZmEXPA9* did not show significant changes after 7 days (Fig. 7C, E, F).

Discussion

Plant organ growth and development are intricately regulated by the redox state, involving key proteins, such as RBOH, NADH oxidase, TOR, and plasma membrane H$^+$-ATPases [45, 46], alongside hormonal and sugar signaling [47]. Several studies highlight the relationship between the redox state and the regulation of plant organ growth and development [14, 20].

Humic acids are well-documented in the literature for their chemical structure and biological activity as biostimulants [6, 28, 29, 31, 33, 48]. However, many aspects of their effects and underlying mechanisms remain unclear. Chemical analysis of the HA revealed molecules from CAS, carboxylic acids, and lignin groups, indicative of conjugated polycyclic aromatic quinone, phenolic, and heterocyclic groups, possibly of fungal/microbial origin, similar to HAs from soil and lignite [48]. The observed root structure modifications likely involve ROS modulation mediated by the presence of quinones and flavonoid-like structures. Gayomba and Muday (2020) [49] observed that root hair-forming cells exhibit increased expression of RBOHC and higher ROS levels. In RBOHC mutants, auxin-induced root hair initiation is reduced, while mutants with elevated flavonoid production show enhanced root hair formation. This suggests that flavonoids play a critical role in regulating root development by modulating ROS accumulation. We

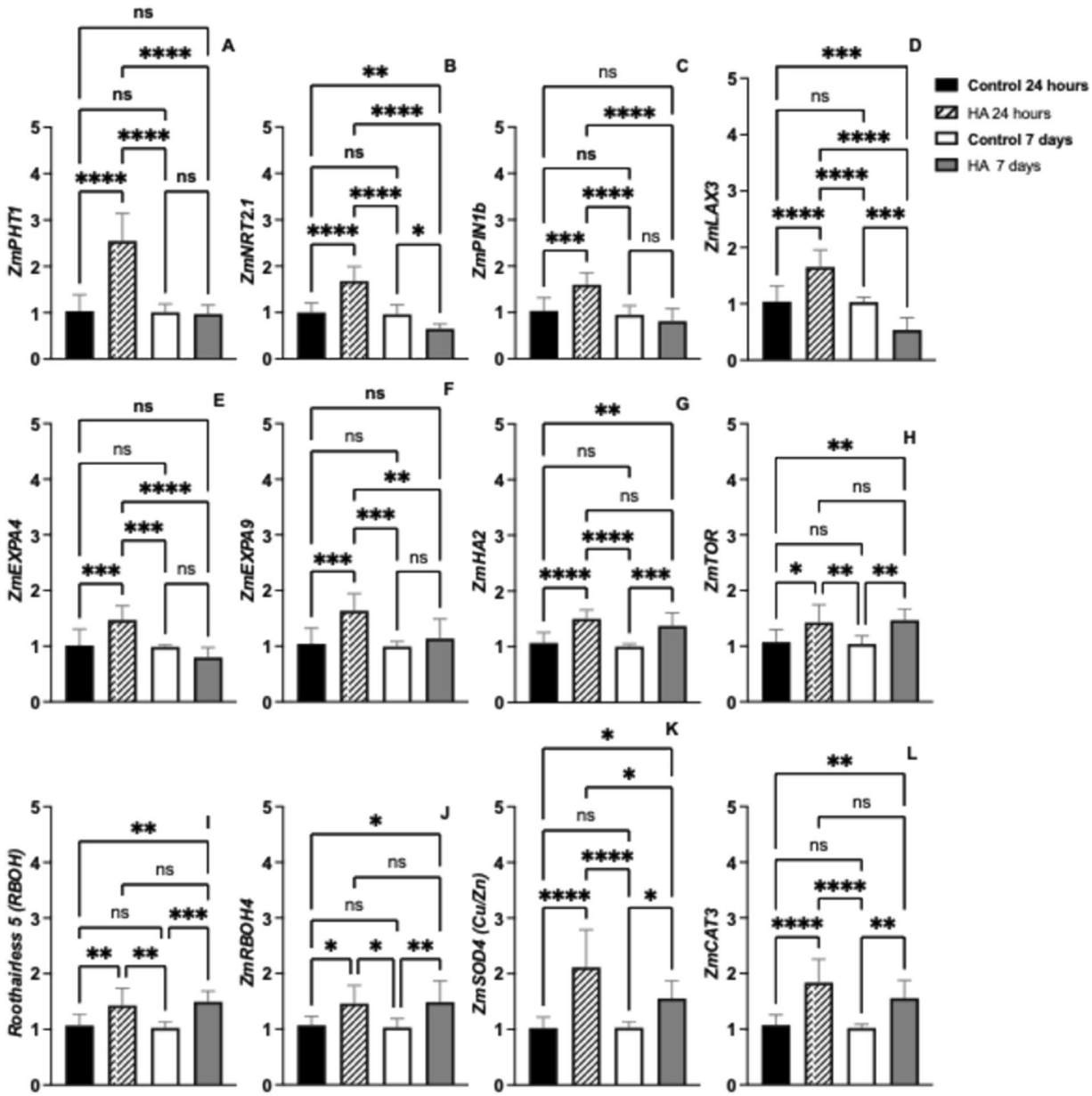

Fig. 7 Gene expression analyses were conducted in plant roots at 24 h and 7 days following HA treatment. **A** *Zea mays high-affinity phosphate transporter1* (*ZmPHT1*); **B** *Zea mays* high-affinity nitrate transport 2.1 (*ZmNRT2.1*); **C** *Zea mays PIN-FORMED auxin transporter1b* (*ZmPIN1b*); **D** *Zea mays high-affinity auxin influx carrier3* (*ZmLAX3*); **E** *Zea mays* expansin-related genes 4 (*ZmEXPA4*); **F** *Zea mays* expansin-related genes9 (*ZmEXPA9*); **G** *Zea mays* plasma membrane H^+-ATPase2 (*ZmHA2*); **H** *Zea mays Target of rapamycin* (*ZmTOR*); **I** *Zea mays Roothairless5 (RTH5–RBOH)*; **J** *Zea mays respiratory burst oxidase homologs D* (*ZmRBOH4*); **K** *Zea mays copper, zinc-superoxide dismutase 4* (*ZmSODCu/Zn4*) and **L** *Zea mays* Catalase3 (*ZmCAT3*). Asterisks indicate significant differences according to Tukey's test (*P < 0.05, **P < 0.01, ***P < 0.001, ****P < 0.0001, ns = not significant)

observed a modulation of ROS levels, likely due to the activity of antioxidant enzymes and non-enzymatic pathways. Furthermore, the polyphenols present in the HA have also contributed to ROS modulation.

Quinones, present in HS, have notable effects on plant growth. By acting as pro-oxidants, they can positively influence growth, particularly at low concentrations. Flaig and Saalbach (1955) [50] observed enhanced germination in cereal seeds when minimal concentrations of thymoquinone and thymohydroquinone were applied, suggesting that quinones impact respiration via the redox system. Because respiration is regulated by both photosynthesis and oxidative stress, results revealed that both processes were positively affected by HA application.

Specifically, HA treatment increased the effective quantum yield and the redox state of quinone A, while reducing non-photochemical quenching, implying that more energy is directed toward photosynthesis with less energy lost to non-photochemical processes, such as heat dissipation. HA also enhanced the SPAD index (chlorophyll content) and steady-state proton flux, parameters directly linked to efficient light capture and conversion into chemical energy in PSII.

Previous studies have also demonstrated that HA can improve the effective quantum yield of PSII, though primarily under drought stress conditions [51]. HA can stimulate photosynthesis by increasing nitrogen levels and chlorophyll content in leaves [52]. Here, it was observed that HA alone can modify both effective quantum yield of PSII and the electron transport across the thylakoid membrane, thereby influencing proton motive force and ATP synthesis. A causal relationship between root acidification and increase in photosynthesis was suggested in *Vigna unguiculata* L. [53]. The observed increase in fine root development, along with enhanced H^+-ATPase activity, supports the hypothesized link between rhizosphere acidification and improved photosynthetic efficiency.

The detection of naphthoquinones in the sample, including 3,3′-bisjuglone, suggests a potential role in the activation of plant defense responses. Van Gestelen et al. (1998) [54] found that compounds such as juglone, 1,4-naphthoquinone, and 2,3-dichloro-1,4-naphthoquinone significantly enhanced $O_2^{\bullet -}$ production mediated by NAD(P)H-dependent enzymes. Their study demonstrated that juglone is reduced to its semiquinone form by NAD(P)H. Conversely, plant quinone reductases (QRs) protect against quinone-induced oxidative damage, as demonstrated by a study, where overexpression of a mitochondrial QR improved growth and photosynthesis under heat stress [55]. Quinone reductases can use both NADH and NADPH as electron sources to catalyze the formation of a reduced hydroquinone, transferring two electrons to a quinone rather than creating the more reactive, one-electron reduced semiquinone [56]. This action may help maintain redox homeostasis, ultimately supporting plant acclimatization and growth. The observed effects on root growth and development likely result from interactions between HA's pro-oxidant properties (e.g., quinones and semiquinone radicals) and its antioxidant components, such as polyphenols [57].

Rapid production of ROS is promptly mitigated by antioxidant activity [27, 49], serving as an early signal for stress detection and activates downstream signal transduction pathways [27]. This study showed that HA induces a transient increase in $O2^{\bullet -}$, likely due to enhanced NADPH oxidase (RBOH) activity. H^+-ATPase activities, NADH oxidase, and antioxidant activities together contribute to maintaining cellular redox balance. The activities of RBOH and NADH oxidase release protons into the cytoplasm, lowering cytoplasmic pH, which can activate plasma membrane H^+-ATPases [58]. Here we provide the first evidence that root growth stimulation involves the combined activities of NADH oxidase, associated with plasma membrane extension [12], and the coordinated interaction between RBOH and H^+-ATPase, wherein proton efflux mediated by H^+-ATPase and RBOH-derived ROS in the apoplast contribute to cell wall loosening during root development [46]. In addition, co-regulation of RBOH and H^+-ATPase at the transcriptional level has been observed, with evidence that H_2O_2 and Ca^{2+} can regulate the expression of both genes [59]. Accordingly, HA increased cytosolic calcium transients and ROS wave in Arabidopsis roots [31].

The increase in H_2O_2 may activate HPCA1 (HYDROGEN- PEROXIDE-INDUCED Ca^{2+} INCREASES), a leucine-rich repeat receptor kinase (LRR-RK) located on the cell surface that enhances Ca^{2+} signaling [60, 61]. HPCA1 is distributed throughout the root system, including in root hairs, emphasizing its role in regulating cell elongation through auxin-mediated pathways [61, 62]. Interestingly, HPCA1 is also involved in plant responses to quinones [63], though the specific connection between quinones, ROS, and HPCA1 in root development remains unclear. Given that Ca^{2+} modulates various signaling pathways, the interaction between HPCA1, RBOH, and apoplastic H_2O_2 accumulation likely plays a role in modulating root development [62, 64]. Our findings are in line with the *HPCA1* and *RBOHC* upregulation in Arabidopsis roots treated with HA [31].

In this study, corn roots experienced oxidative stress shortly after HA application, followed by a significant increase in antioxidant activity through SOD, CAT, and total non-enzymatic antioxidant capacity within a few hours. Similarly, HA from different sources has been shown to stimulate CAT and SOD activity in other plant species [64, 65]. Increased transcript levels of *ZmSOD4* and *ZmCAT3* were also observed in plants treated with HA. *ZmSOD4* is a maize isoform highly expressed in response to abiotic stress and abscisic acid (ABA) treatment [66, 67], while *ZmCAT3* is upregulated in roots in response to auxin and H_2O_2 treatments [68, 69]. The apoplastic enzyme Cu/Zn SOD can utilize protons extruded into the apoplast by H^+-ATPase to dismutate $O_2^{\bullet -}$ to H_2O_2. This process reflects a coordinated action between Cu/Zn SOD, RBOH, and H^+-ATPase [46, 70]. Detoxification of H_2O_2 occurs through peroxidase activity in the apoplast, which breaks down H_2O_2 using electron donors, such as phenolics and flavonoids

[71]. Meanwhile, H_2O_2 can also enter the cell via aquaporins and is subsequently detoxified in the cytoplasm by catalases [72]. These results suggest that HA induces a transient oxidative stress, which is subsequently counterbalanced by an increase in antioxidant responses. This balance may be a critical factor in determining the optimal timing and frequency of HA applications in the field.

HA from different sources regulates lateral root number and root hair formation in various plant species [30, 48]. The results of this study link HA with ROS signaling, ultimately connecting them to enhanced root growth, particularly through increased lateral roots and the development of finer root structures, which improve the plant's nutrient foraging capacity. A greater number of fine roots can enhance the nutrient use efficiency of plants by increasing their absorptive capacity, thereby enabling the use of less fertilizer to achieve the same level of productivity. In nutrient-deficient soils, the expanded absorptive area provided by finer root structures can particularly improve plant performance [73].

Humic acids enhance soil P solubilization, mobility and increase the expression and activity of H^+-ATPase, all of which contribute to promoting P uptake [74]. The high-affinity phosphate transporter *ZmPHT1* is responsible for inorganic phosphate uptake from the soil and its redistribution within plants [75]. Furthermore, HA increased the expression of phosphate-related genes (*ZmPHT1*) after 24 h, potentially contributing to a greater number of transporters and enhancing the plant's phosphate absorption. In addition, HA was observed to increase the expression of the high-affinity nitrate transporter *ZmNRT2.1*, suggesting a potential increase in nitrogen uptake, as reflected by the higher SPAD index. The transient induction observed for most evaluated genes after HA application has significant implications for understanding its mode of action. This rapid yet temporary upregulation of genes, such as those involved in nutrient uptake, suggests that the timing of HA application could be critical for maximizing its beneficial effects on plant physiology.

Plants treated with HA also showed increased transcript levels of *Roothairless5* (*RTH5*) after 24 h, which plays a crucial role in the development of root hairs in maize. *RTH5* transcripts accumulate in roots, with the highest levels detected in root hairs [76]. This gene is closely related to the *AtRBOH* family, which is essential for establishing peaks of $O_2^{\bullet -}$ and H_2O_2 and maintaining elevated Ca^{2+} levels in the tips of growing root hairs [76]. Interestingly, another gene from the *RBOH* family, *ZmRBOH4*, was induced by HA treatment after 24 h. This gene plays a role in plant immunity by initiating oxidative bursts in response to pathogen attacks and contributes to maize's resistance to gray leaf spot [77]. The functional similarity suggests that *ZmRBOH4* is an ortholog of *AtRBOHD* [77], which is also integral to the plant immune response and plays a critical role in the oxidative burst that occurs upon pathogen attack in *Arabidopsis thaliana* [78].

In addition, HA improve *ZmHA2* gene expression (Fig. 7G) in maize roots. ZmHA2 is an important and the most abundant isoform, expressed in different tissues, present in phloem cells, stomatal guard cells and root epidermis [79], and also is correlated with nitrate uptake by *ZmNRT2.1* [80]. Consistent with this, both *ZmHA2* and *ZmNRT2.1* are affected by HA from earthworm casting [81]. Furthermore, our findings show that HA also promoted increased expression of *Target of Rapamycin (TOR)*, a key gene in plant development. This observation aligns with a very recent report in Arabidopsis roots [31] demonstrating that HA upregulates both *H^+-ATPase (AHA2)* and *TOR kinase*, leading to H^+-ATPase-dependent TOR signaling activation. Supporting this link, a correlation between H^+-ATPase and TOR protein complex 1 (TORC1) activity has also been shown in *Nicotiana tabacum* cells, where H^+-ATPase activation induced TORC1 activity even under nutrient- and auxin-free conditions [45]. The TORC1, serves as a central regulatory hub integrating diverse internal and external signals related to plant growth, development, and stress responses, influencing numerous processes, such as photosynthesis, nutrient absorption, fruit development, and interactions with microorganisms [82].

ROS, nitric oxide (NO), and auxin are known to play key roles in promoting root growth and development [83]. Our observation in this study corroborates the HA-mediated stimulation of root development (Fig. 4) involving NO and interaction with plasma membrane H^+-ATPase, a phenomenon first described by [30]. Interestingly, NO can enhance RBOH activity through S-nitrosylation, leading to increased production of $O_2^{\bullet -}$ [84]. It was observed that HA increase NO concentration over several hours, enhance H^+-ATPase activity, and boosted the expression of auxin-related genes, such as the efflux carrier *PIN1b* and the influx carrier *LAX3*, after 24 h of treatment. Trevisan et al. (2010) [85] also demonstrated that HA induces the auxin pathway, as shown by the auxin synthetic reporter DR5::GUS and the increased transcription of auxin-responsive genes. In fact, HA from a sedimentary source increases auxin concentration in roots [86], which in turn could trigger auxin response pathways.

ROS can alter auxin biosynthesis, metabolism, and signaling [21], while auxin can also influence ROS production [87, 88], further highlighting the interaction between ROS and auxin-mediated signaling. The putative ortholog of *AtPIN1* in *Zea mays*, *PIN-formed 1b* (*ZmPIN1b*), mediates auxin transport in maize roots. In

Arabidopsis thaliana, it has been shown that *PIN* genes play a critical role in root growth and development [60]. *ZmPIN1b* is differentially expressed in maize vegetative and reproductive tissues and during kernel development. It plays a fundamental role in meristem function, indicating the involvement of internal tissues in organ positioning [50, 89]. Upregulation of *ZmPIN1b* has been shown to promote the growth of both lateral and seminal roots, as observed in this study [90]. A positive correlation between auxin and ROS in orchestrating cell division and regulating auxin flux through PIN proteins during root development, as found in this study, was also demonstrated by [91]. The auxin influx transporter *LAX* genes, which are paralogs of *AUX1*, are directly correlated with the induction of lateral root emergence in *Arabidopsis thaliana* [92]. Modulation of *ZmLAX3* and other *LAX* genes has been analyzed in corn under various abiotic stresses [74]. Nevertheless, the role of this isoform in root development has yet to be fully established.

HA also increased the transcription of two important genes related to cell expansion, *ZmEXP4* and *ZmEXP9.* Both encode expansins, which are proteins involved in loosening the bonds between cell wall polysaccharides during the cell elongation process [93]. The mode of action of HS is founded in the plasma membrane H^+-ATPase activation [30, 81], but remained to be shown if the pH reduction on the apoplast resulting in cell wall loosening would affect the expansins. The genes *ZmEXPA4* and *ZmEXPA9*, along with *ZmPIN1b* and *ZmLAX3*, are associated with apoplastic acidification resulting from auxin signaling-mediated H^+ pumping and the activation of plasma membrane H^+-ATPase. We believe that the HA transiently change the cell wall pH resulting in the wall loosening by expansins (*ZmEXPA4* and *ZmEXPA9*), that requires auxin transporters transcription (*ZmPIN1b* and *ZmLAX3*). The upregulation of these genes highlights the role of auxin signaling in the HA-induced development of more highly branched root systems.

Conclusions

The redox-associated enzymes NADH oxidase and RBOH appear to play central roles in the mechanism of HA action, which involves ROS, NO, and auxin signaling. The HA-induced accumulation of ROS and NO is correlated with the activation of the H^+ pump and modulation of the auxin transport pathway, potentially promoting root development through the acid growth process. Consequently, HA-induced modifications in root architecture, potentially alongside direct effects on photobiology, lead to increased lateral root formation and finer root development. These architectural changes enhance the plant's foraging capacity, which can subsequently improve nutrient uptake. The oxidative bursts induced by HA are counterbalanced by the activation of antioxidant responses, suggesting that these organic compounds may act as drivers of redox modulation. Furthermore, to complete this scenario, bioactive components of HA, such as small quinone-like compounds and flavonoid structures, are likely contributors to these processes. Further research is needed to fully elucidate the effects of temporal applications to both roots and leaves on nutrient uptake and transport efficiency, as well as their broader implications for crop yield and soil health.

Supplementary Information

The online version contains supplementary material available at https://doi.org/10.1186/s40538-025-00789-9.

Additional file 1.

Acknowledgements
A portion of this work was performed at the National High Magnetic Field Laboratory, which is supported by the National Science Foundation Division of Chemistry and Division of Materials Research through Cooperative Agreement No. DMR-1644779 and the state of Florida. We thank HUMA Inc. for financial support.

Author contributions
D.B.Z., M.P.S., R.T.L.: conceptualization; D.B.Z., M.P.S., R.T.L.: methodology; D.B.Z., M.P.S., R.T.L., J.G.,: formal analysis; D.B.Z., M.P.S., J.G., A.J., H.M.: investigation; R.T.L.: resources; D.B.Z., M.P.S., R.T.L.: data curation; D.B.Z., M.P.S.: writing—original draft; D.B.Z., M.P.S., R.T.L.: writing—review and editing; D.B.Z., M.P.S., H.M.,: visualization; D.B.Z., M.P.S., R.T.L.: supervision; R.T.L.: funding acquisition

Funding
The work was supported by Huma, Inc.

Availability of data and materials
No datasets were generated or analysed during the current study.

Declarations

Ethics approval and consent to participate
This manuscript is original and has not been published in other journals. The authors agreed to keep the copyright rule.

Consent for publication
The authors agreed to the publication of the manuscript in this journal.

Competing interests
The authors declare no competing interests.

Author details
[1]Instituto de Biodiversidade E Sustentabilidade, Universidade Federal Do Rio de Janeiro, Rio de Janeiro, Brazil. [2]Huma Inc, Gilbert, AZ, USA.

Received: 28 February 2025 Accepted: 13 May 2025
Published online: 30 May 2025

References

1. Hayes MHB, Swift RS. Chapter One - Vindication of humic substances as a key component of organic matter in soil and water. In: Sparks DL, editor. Academic Press; 2020. p. 1–37. (Advances in Agronomy; vol. 163). Available from: https://www.sciencedirect.com/science/article/pii/S0065211320300468

2. Piccolo A, Drosos M. The essential role of humified organic matter in preserving soil health. Chem Biol Technol Agric. 2025;12(1):21.
3. Lamar RT, Gralian J, Hockaday WC, Jerzykiewicz M, Monda H. Investigation into the role of carboxylic acid and phenolic hydroxyl groups in the plant biostimulant activity of a humic acid purified from an oxidized subbituminous coal. Front Plant Sci. 2024. https://doi.org/10.3389/fpls.2024.1328006.
4. Olk DC, Dinnes DL, Rene Scoresby J, Callaway CR, Darlington JW. Humic products in agriculture: potential benefits and research challenges—a review. J Soils Sediments. 2018;18:2881–91.
5. Olk D, Dinnes D, Hatfield R, Scoresby J, Darlington J. Variable humic product effects on maize structural biochemistry across annual weather patterns and soil types in two Iowa (USA) production fields. Front Plant Sci. 2023;13:1058141.
6. Zandonadi DB, Santos MP, Busato JG, Peres LEP, Façanha AR. Plant physiology as affected by humified organic matter. Theor Exp Plant Physiol. 2013;25:13–25.
7. Zandonadi DB, Santos MP, Medici LO, Silva J. Ação da matéria orgânica e suas frações sobre a fisiologia de hortaliças. Hortic Bras. 2014;32(1):14–20.
8. Bridge A, Barr R, Morré DJ. The plasma membrane NADH oxidase of soybean has vitamin K1 hydroquinone oxidase activity. Biochim Biophys Acta BBA-Biomembr. 2000;1463(2):448–58.
9. Jiménez-Quesada MJ, Traverso JÁ, de Alché JD. NADPH oxidase-dependent superoxide production in plant reproductive tissues. Front Plant Sci. 2016;7:359.
10. Morré D, Navas P, Penel C, Castillo F. Auxin-stimulated NADH oxidase (semidehydroascorbate reductase) of soybean plasma membrane: role in acidification of cytoplasm? Protoplasma. 1986;133:195–7.
11. Brightman AO, Barr R, Crane FL, Morré DJ. Auxin-stimulated NADH oxidase purified from plasma membrane of soybean. Plant Physiol. 1988;86(4):1264–9.
12. Brightman AO, Morré DJ. NADH oxidase of the plasma membrane of plants. Oxidoreduct Plasma Membr Relat Growth Transp. 1991;2:85–110.
13. Morré DJ. The role of NADH oxidase in growth and physical membrane displacement. Protoplasma. 1995;184:14–21.
14. Ali MF, Muday GK. Reactive oxygen species are signaling molecules that modulate plant reproduction. Plant Cell Environ. 2024;47(5):1592–605.
15. Zhang X, Bian A, Li T, Ren L, Li L, Su Y, et al. ROS and calcium oscillations are required for polarized root hair growth. Plant Signal Behav. 2022;17(1):2106410.
16. Lherminier J, Elmayan T, Fromentin J, Elaraqui KT, Vesa S, Morel J, et al. NADPH oxidase-mediated reactive oxygen species production: subcellular localization and reassessment of its role in plant defense. Mol Plant Microbe Interact. 2009;22(7):868–81.
17. Zhang H, Wang X, Yan A, Deng J, Xie Y, Liu S, et al. Evolutionary analysis of respiratory burst oxidase homolog (RBOH) genes in plants and characterization of ZmRBOHs. Int J Mol Sci. 2023;24(4):3858.
18. Guadagno CR, Ewers BE, Weinig C. Circadian rhythms and redox state in plants: till stress do us part. Front Plant Sci. 2018;9:247.
19. Martin RE, Postiglione AE, Muday GK. Reactive oxygen species function as signaling molecules in controlling plant development and hormonal responses. Curr Opin Plant Biol. 2022;69: 102293.
20. Considine MJ, Foyer CH. Oxygen and reactive oxygen species-dependent regulation of plant growth and development. Plant Physiol. 2021;186(1):79–92.
21. Tognetti VB, Bielach A, Hrtyan M. Redox regulation at the site of primary growth: auxin, cytokinin and ROS crosstalk. Plant Cell Environ. 2017;40(11):2586–605.
22. Hashimoto T, Hashimoto K, Shindo H, Tsuboyama S, Miyakawa T, Tanokura M, et al. Enhanced Ca2+ binding to EF-hands through phosphorylation of conserved serine residues activates MpRBOHB and chitin-triggered ROS production. Physiol Plant. 2023;175(6): e14101.
23. Ravi B, Foyer CH, Pandey GK. The integration of reactive oxygen species (ROS) and calcium signalling in abiotic stress responses. Plant Cell Environ. 2023;46(7):1985–2006.
24. Waszczak C, Akter S, Jacques S, Huang J, Messens J, Van Breusegem F. Oxidative post-translational modifications of cysteine residues in plant signal transduction. J Exp Bot. 2015;66(10):2923–34.
25. Smirnoff N, Arnaud D. Hydrogen peroxide metabolism and functions in plants. New Phytol. 2019;221(3):1197–214.
26. Sanchez-Corrionero A, Sánchez-Vicente I, Arteaga N, Manrique-Gil I, Gómez-Jiménez S, Torres-Quezada I, et al. Fine-tuned nitric oxide and hormone interface in plant root development and regeneration. J Exp Bot. 2023;74(19):6104–18.
27. Mittler R, Zandalinas SI, Fichman Y, Van Breusegem F. Reactive oxygen species signalling in plant stress responses. Nat Rev Mol Cell Biol. 2022;23(10):663–79.
28. Nardi S, Muscolo A, Vaccaro S, Baiano S, Spaccini R, Piccolo A. Relationship between molecular characteristics of soil humic fractions and glycolytic pathway and krebs cycle in maize seedlings. Soil Biol Biochem. 2007;39(12):3138–46.
29. Rathor P, Upadhyay P, Ullah A, Gorim LY, Thilakarathna MS. Humic acid improves wheat growth by modulating auxin and cytokinin biosynthesis pathways. AoB Plants. 2024;16(2):plae018.
30. Zandonadi DB, Santos MP, Dobbss LB, Olivares FL, Canellas LP, Binzel ML, et al. Nitric oxide mediates humic acids-induced root development and plasma membrane H+-ATPase activation. Planta. 2010;231:1025–36.
31. Santos MP, Zupunski M, Monda H, Gralian J, James A, Grossmann G, et al. Humic acids modify root architecture in Arabidopsis through H+-ATPase-dependent target of rapamycin activation in concert with Ca2+ and ROS signaling. Chem Biol Technol Agric. 2025;12(1):47.
32. Zandonadi DB, Matos CRR, Castro RN, Spaccini R, Olivares FL, Canellas LP. Alkamides: a new class of plant growth regulators linked to humic acid bioactivity. Chem Biol Technol Agric. 2019;6:1–12.
33. Canellas LP, Canellas NO, da Irineu LESS, Olivares FL, Piccolo A. Plant chemical priming by humic acids. Chem Biol Technol Agric. 2020;7:1–17.
34. Lamar RT, Olk DC, Mayhew L, Bloom PR. Determination of humic and fulvic acids in commercial solid and liquid humic products by alkaline extraction and gravimetric determination. J AOAC Int. 2014;97(3):721–30.
35. Blakney GT, Hendrickson CL, Marshall AG. Predator data station: A fast data acquisition system for advanced FT-ICR MS experiments. Int J Mass Spectrom. 2011;306(2–3):246–52.
36. Kaiser NK, Savory JJ, Hendrickson CL. Controlled ion ejection from an external trap for extended m/z range in FT-ICR mass spectrometry. J Am Soc Mass Spectrom. 2014;25(6):943–9.
37. Rostad CE, Leenheer JA. Factors that affect molecular weight distribution of Suwannee river fulvic acid as determined by electrospray ionization/mass spectrometry. Anal Chim Acta. 2004;523(2):269–78.
38. KREvELEN V. Graphical-statistical method for the study of structure and reaction processes of coal. Fuel. 1950;29:269–84.
39. Kanazawa A, Chattopadhyay A, Kuhlgert S, Tuitupou H, Maiti T, Kramer DM. Light potentials of photosynthetic energy storage in the field: what limits the ability to use or dissipate rapidly increased light energy? R Soc Open Sci. 2021;8(12): 211102.
40. Bradford MM. A rapid and sensitive method for the quantitation of microgram quantities of protein utilizing the principle of protein-dye binding. Anal Biochem. 1976;72(1–2):248–54.
41. Fiske CH, Subbarow Y. The colorimetric determination of phosphorus. J Biol Chem. 1925;66(2):375–400.
42 Sagi M, Fluhr R. Superoxide production by plant homologues of the gp91phox NADPH oxidase. Modulation of activity by calcium and by tobacco mosaic virus infection. Plant Physiol. 2001;126(3):1281–90.
43. Morré DJ. NADH oxidase activity of soybean plasma membranes inhibited by submicromolar concentrations of ATP. Mol Cell Biochem. 1998;187:41–6.
44 Livak KJ, Schmittgen TD. Analysis of relative gene expression data using real-time quantitative PCR and the 2− ΔΔCT method. Methods. 2001;25(4):402–8.
45. Primo C, Navarre C, Chaumont F, André B. Plasma membrane H+-ATPases promote TORC1 activation in plant suspension cells. iScience. 2022;25(5):104238.
46. Majumdar A, Kar RK. Congruence between PM H+-ATPase and NADPH oxidase during root growth: a necessary probability. Protoplasma. 2018;255:1129–37.
47. Sablowski R, Carnier DM. Interplay between cell growth and cell cycle in plants. J Exp Bot. 2014;65(10):2703–14.
48. Vitti A, Coviello L, Nuzzaci M, Vinci G, Deligiannakis Y, Giannakopoulos E, et al. Biostimulation of humic acids on *Lepidium sativum* L. regulated

by their content of stable phenolic O radicals. Chem Biol Technol Agric. 2024;11(1):92.
49. Gayomba SR, Muday GK. Flavonols regulate root hair development by modulating accumulation of reactive oxygen species in the root epidermis. Development. 2020;147(8):185819.
50. Flaig W, Saalbach E. Humic acids. XI. The effect on germination of cereals of thymohydroquinone as model substance of pre-humic acids or decomposition products of humic acid. 1955;
51. Shen J, Guo MJ, Wang YG, Yuan XY, Wen YY, Song XE, et al. Humic acid improves the physiological and photosynthetic characteristics of millet seedlings under drought stress. Plant Signal Behav. 2020;15(8):1774212.
52. de Castro TAT, Berbara RLL, Tavares OCH, da Graca Mello DF, Pereira EG, de Souza CCB, et al. Humic acids induce a eustress state via photosynthesis and nitrogen metabolism leading to a root growth improvement in rice plants. Plant Physiol Biochem. 2021;162:171–84.
53 Rao TP, Yano K, Iijima M, Yamauchi A, Tatsumi J. Regulation of rhizosphere acidification by photosynthetic activity in cowpea (*Vigna unguiculata* L. Walp.) seedlings. Ann Bot. 2002;89(2):213–20.
54. Van Gestelen P, Asard H, Horemans N, Caubergs RJ. Superoxide-producing NAD (P) H oxidases in plasma membrane vesicles from elicitor responsive bean plants. Physiol Plant. 1998;104(4):653–60.
55. Cheng B, Zhou M, Tang T, Hassan MJ, Zhou J, Tan M, et al. A Trifolium repens flavodoxin-like quinone reductase 1 (TrFQR1) improves plant adaptability to high temperature associated with oxidative homeostasis and lipids remodeling. Plant J. 2023;115(2):369–85.
56 Iyanagi T, Yamazaki I. One-electron-transfer reactions in biochemical systems V. Difference in the mechanism of quinone reduction by the NADH dehydrogenase and the NAD (P) H dehydrogenase (DT-diaphorase). Biochim Biophys Acta BBA-Bioenerg. 1970;216(2):282–94.
57. Monda H, McKenna AM, Fountain R, Lamar RT. Bioactivity of humic acids extracted from shale ore: molecular characterization and structure-activity relationship with tomato plant yield under nutritional stress. Front Plant Sci. 2021;12: 660224.
58. Bobik K, Boutry M, Duby G. Activation of the plasma membrane H+-ATPase by acid stress: antibodies as a tool to follow the phosphorylation status of the penultimate activating Thr. Plant Signal Behav. 2010;5(6):681–3.
59. Majumdar A, Kar RK. Transcriptional co-regulation of plasma membrane H+-ATPase and NADPH oxidase during root growth. Plant Gene. 2021;26: 100272.
60. Fichman Y, Zandalinas SI, Peck S, Luan S, Mittler R. HPCA1 is required for systemic reactive oxygen species and calcium cell-to-cell signaling and plant acclimation to stress. Plant Cell. 2022;34(11):4453–71.
61. Wu F, Chi Y, Jiang Z, Xu Y, Xie L, Huang F, et al. Hydrogen peroxide sensor HPCA1 is an LRR receptor kinase in Arabidopsis. Nature. 2020;578(7796):577–81.
62. Lopez LE, Ibeas MA, Diaz Dominguez G, Estevez JM. Exploring the puzzle of reactive oxygen species acting on root hair cells. J Exp Bot. 2024;75(15):4589–98.
63. Laohavisit A, Wakatake T, Ishihama N, Mulvey H, Takizawa K, Suzuki T, et al. Quinone perception in plants via leucine-rich-repeat receptor-like kinases. Nature. 2020;587(7832):92–7.
64. Tarkowski ŁP, Signorelli S, Considine MJ, Montrichard F. Integration of reactive oxygen species and nutrient signalling to shape root system architecture. Plant Cell Environ. 2023;46(2):379–90.
65. Cordeiro FC, Santa-Catarina C, Silveira V, De Souza SR. Humic acid effect on catalase activity and the generation of reactive oxygen species in corn (Zea mays). Biosci Biotechnol Biochem. 2011;75(1):70–4.
66. Yan J, Li J, Zhang H, Liu Y, Zhang A. ZmWRKY104 positively regulates salt tolerance by modulating ZmSOD4 expression in maize. Crop J. 2022;10(2):555–64.
67. Zhu Y, Liu W, Sheng Y, Zhang J, Chiu T, Yan J, et al. ABA affects brassinosteroid-induced antioxidant defense via ZmMAP65-1a in Maize plants. Plant Cell Physiol. 2015;56(7):1442–55.
68 Polidoros AN, Scandalios JG. Role of hydrogen peroxide and different classes of antioxidants in the regulation of catalase and glutathione S-transferase gene expression in maize (*Zea mays* L.). Physiol Plant. 1999;106(1):112–20.
69. Guan LM, Scandalios JG. Catalase gene expression in response to auxin-mediated developmental signals. Physiol Plant. 2002;114(2):288–95.
70 Majumdar A, Kar RK. Orchestration of Cu-Zn SOD and class III peroxidase with upstream interplay between NADPH oxidase and PM H+-ATPase mediates root growth in *Vigna radiata* (L.) Wilczek. J Plant Physiol. 2019;232:248–56.
71. Yamasaki H, Sakihama Y, Ikehara N. Flavonoid-peroxidase reaction as a detoxification mechanism of plant cells against H2O2. Plant Physiol. 1997;115(4):1405–12.
72. Bienert GP, Schjoerring JK, Jahn TP. Membrane transport of hydrogen peroxide. Biochim Biophys Acta BBA-Biomembr. 2006;1758(8):994–1003.
73. Wu X, Li H, Rengel Z, Whalley WR, Li H, Zhang F, et al. Localized nutrient supply can facilitate root proliferation and increase nitrogen-use efficiency in compacted soil. Soil Tillage Res. 2022;215: 105198.
74. Yuan Y, Tang C, Jin Y, Cheng K, Yang F. Contribution of exogenous humic substances to phosphorus availability in soil-plant ecosystem: a review. Crit Rev Environ Sci Technol. 2023;53(10):1085–102.
75. Victor Roch G, Maharajan T, Ceasar SA, Ignacimuthu S. The role of PHT1 family transporters in the acquisition and redistribution of phosphorus in plants. Crit Rev Plant Sci. 2019;38(3):171–98.
76. Nestler J, Liu S, Wen T, Paschold A, Marcon C, Tang HM, et al. Roothairless5, which functions in maize (*Zea mays* L.) root hair initiation and elongation encodes a monocot-specific NADPH oxidase. Plant J. 2014;79(5):729–40.
77. Zhong T, Zhu M, Zhang Q, Zhang Y, Deng S, Guo C, et al. The ZmWAKL–ZmWIK–ZmBLK1–ZmRBOH4 module provides quantitative resistance to gray leaf spot in maize. Nat Genet. 2024;56(2):315–26.
78. Kadota Y, Shirasu K, Zipfel C. Regulation of the NADPH oxidase RBOHD during plant immunity. Plant Cell Physiol. 2015;56(8):1472–80.
79. Frías I, Caldeira MT, Pérez-Castiñeira JR, Navarro-Aviñó JP, Culiañez-Maciá FA, Kuppinger O, et al. A major isoform of the maize plasma membrane H (+)-ATPase: characterization and induction by auxin in coleoptiles. Plant Cell. 1996;8(9):1533–44.
80. Santi S, Locci G, Monte R, Pinton R, Varanini Z. Induction of nitrate uptake in maize roots: expression of a putative high-affinity nitrate transporter and plasma membrane H+-ATPase isoforms. J Exp Bot. 2003;54(389):1851–64.
81 Quaggiotti S, Ruperti B, Pizzeghello D, Francioso O, Tugnoli V, Nardi S. Effect of low molecular size humic substances on nitrate uptake and expression of genes involved in nitrate transport in maize (*Zea mays* L.). J Exp Bot. 2004;55(398):803–13.
82. Rabeh K, Oubohssaine M, Hnini M. TOR in plants: Multidimensional regulators of plant growth and signaling pathways. J Plant Physiol. 2024;294: 154186.
83 Gupta DK, Palma JM, Corpas FJ. Nitric oxide and hydrogen peroxide signaling in higher plants. Springer; 2019.
84. Samant SB, Yadav N, Swain J, Joseph J, Kumari A, Praveen A, et al. Nitric oxide, energy, and redox-dependent responses to hypoxia. J Exp Bot. 2024;75(15):4573–88.
85. Trevisan S, Pizzeghello D, Ruperti B, Francioso O, Sassi A, Palme K, et al. Humic substances induce lateral root formation and expression of the early auxin-responsive IAA19 gene and DR5 synthetic element in Arabidopsis. Plant Biol. 2010;12(4):604–14.
86. Mora V, Baigorri R, Bacaicoa E, Zamarreno AM, García-Mina JM. The humic acid-induced changes in the root concentration of nitric oxide, IAA and ethylene do not explain the changes in root architecture caused by humic acid in cucumber. Environ Exp Bot. 2012;76:24–32.
87. Krishnamurthy A, Rathinasabapathi B. Oxidative stress tolerance in plants: novel interplay between auxin and reactive oxygen species signaling. Plant Signal Behav. 2013;8(10): e25761.
88. Morré DJ, Morré DM, Ternes P. Auxin-activated NADH oxidase activity of soybean plasma membranes is distinct from the constitutive plasma membrane NADH oxidase and exhibits prion-like properties. Vitro Cell Dev Biol-Plant. 2003;39:368–76.
89. Carraro N, Forestan C, Canova S, Traas J, Varotto S. ZmPIN1a and ZmPIN1b encode two novel putative candidates for polar auxin transport and plant architecture determination of maize. Plant Physiol. 2006;142(1):254–64.
90. Li Z, Li P, Zhang J. Expression analysis of PIN-formed auxin efflux transporter genes in maize. Plant Signal Behav. 2019;14(9):1632689.
91. Pasternak T, Palme K, Pérez-Pérez JM. Role of reactive oxygen species in the modulation of auxin flux and root development in Arabidopsis thaliana. Plant J. 2023;114(1):83–95.

92. Swarup K, Benková E, Swarup R, Casimiro I, Péret B, Yang Y, et al. The auxin influx carrier LAX3 promotes lateral root emergence. Nat Cell Biol. 2008;10(8):946–54.
93. Cosgrove DJ. Structure and growth of plant cell walls. Nat Rev Mol Cell Biol. 2024;25(5):340–58.

Publisher's Note